frontiers in Chemistry

ORIGINAL RESEARCH
published: 18 February 2020
doi: 10.3389/fchem.2019.00941

Accelerating Photocatalytic Hydrogen Production and Pollutant Degradation by Functionalizing g-C_3N_4 With SnO_2

Amir Zada[2], *Muhammad Khan*[3], *Muhammad Nasimullah Qureshi*[4], *Shu-yuan Liu*[5,6]* *and Ruidan Wang*[1]*

[1] *Institute of Catalysis for Energy and Environment, College of Chemistry and Chemical Engineering, Shenyang Normal University, Shenyang, China,* [2] *Department of Chemistry, Abdul Wali Khan University Mardan, Mardan, Pakistan,* [3] *School of Materials Science and Engineering, Northwestern Polytechnical University, Xi'an, China,* [4] *Department of Chemistry, University of Swabi, Swabi, Pakistan,* [5] *Department of Pharmacology, Shenyang Medical College, Shenyang, China,* [6] *Key Laboratory for Photonic and Electronic Bandgap Materials, Ministry of Education, College of Physics and Electronic Engineering, Harbin Normal University, Harbin, China*

Energy crises and environmental pollution are two serious threats to modern society. To overcome these problems, graphitic carbon nitride (g-C_3N_4) nanosheets were fabricated and functionalized with SnO_2 nanoparticles to produce H_2 from water splitting and degrade 2-chlorophenol under visible light irradiation. The fabricated samples showed enhanced photocatalytic activities for both H_2 evolution and pollutant degradation as compared to bare g-C_3N_4 and SnO_2. These enhanced photoactivities are attributed to the fast charge separation as the excited electrons transfer from g-C_3N_4 to the conduction band of SnO_2. This enhanced charge separation has been confirmed by the photoluminescence spectra, steady state surface photovoltage spectroscopic measurement, and formed hydroxyl radicals. It is believed that this work will provide a feasible route to synthesize photocatalysts for improved energy production and environmental purification.

Keywords: g-C_3N_4, SnO_2, photocatalysis, hydrogen production, organic pollutant

OPEN ACCESS

Edited by:
Liwei Wang,
Guangxi University, China

Reviewed by:
Zhenyi Zhang,
Dalian Nationalities University, China
Qin Li,
South-Central University for Nationalities, China

***Correspondence:**
Shu-yuan Liu
liushuyuan@symc.edu.cn
Ruidan Wang
wangruidan1980@163.com

Specialty section:
This article was submitted to Nanoscience, a section of the journal Frontiers in Chemistry

Received: *12 November 2019*
Accepted: *26 December 2019*
Published: *18 February 2020*

Citation:
Zada A, Khan M, Qureshi MN, Liu S and Wang R (2020) Accelerating Photocatalytic Hydrogen Production and Pollutant Degradation by Functionalizing g-C_3N_4 With SnO_2. Front. Chem. 7:941. doi: 10.3389/fchem.2019.00941

INTRODUCTION

Exhaustion of hydrocarbon fuels and addition of toxic and hazardous materials from agricultural, medicinal, dyes, and cosmetic industries to the environment have resulted in increased pressure on the scientific community to address these problems adequately. A number of methods have been chalked out such as cracking of hydrocarbons and thermal splitting of water at elevated temperature to get H_2 (future fuel). However, these methods require highly costly and controlled operational environment and huge labor under normal conditions. On the other hand, different pollutants removal technologies such as adsorption, coagulation, and electrochemical methods have their own shortcomings and did not receive much popularity in the purification of the environment (Zhao et al., 2015; Gautam et al., 2016; Li et al., 2016; Ali et al., 2018b; Wang et al., 2018; Ali S. et al., 2019). Therefore, modern techniques are urgently required to address energy and environmental issues properly with the least operational cost and time.

Photocatalysis has opened a brilliant chapter to realize the energy crises and environmental issues. The photocatalysts have shown their remarkable influence in the production of H_2 from water, production of hydrocarbon fuels from CO_2, and removal of pollutants from air and

wastewater with minimum cost and least working labor (Singh et al., 2017; Li et al., 2018a,b; Qu et al., 2018; Ullah et al., 2019; Xu et al., 2019a). Although different photocatalysts such as TiO_2, ZnO, and ZrO_2 have been widely utilized, there are some typical problems such as activeness only under ultraviolet (UV) light and fast recombination of photogenerated charges (Raizada et al., 2017; Qi et al., 2018a,b, 2020a). Since visible light contributes a major portion to electromagnetic radiations, therefore, photocatalysts active under visible light are more effective and efficient. Graphitic carbon nitride, g-C_3N_4, is a promising polymeric photocatalyst with a band gap of 2.7 eV. Its conduction band (CB) and valence band (VB) have characteristic abilities to reduce water and oxidize organic pollutants, respectively (Qi et al., 2019a,b). Its metal-free nature is of particular importance as its release to the environment does not produce harmful threats to the aquatic animals and plants (Nie et al., 2018; Ran et al., 2018; Fu et al., 2019; Liu M. et al., 2019). However, low surface area and poor excited charge separation capability of this photocatalyst is still a marked question on its utilization for fuel production and organic oxidation (Dong et al., 2019; Liu Y. et al., 2019; Zhu et al., 2019c; Qi et al., 2020b). Therefore, these problems need to be tackled in future generation of semiconductor photocatalysis.

SnO_2 is an excellent UV responsive metal oxide photocatalyst with a band gap of 3.5 eV. Its excellent stability and tunable optical properties make it a suitable candidate for photocatalysis, solar cells, and gas sensors. More interestingly, its CB is situated at a suitable position below the CB of g-C_3N_4 and thermodynamically acts as a sink to accept the excited electrons from g-C_3N_4 during photocatalysis (Jana and Mondal, 2014; Xu et al., 2018a; Qi et al., 2019c,d). Therefore, its heterojunctional combination with g-C_3N_4 will significantly improve excited charge separation for enhanced photocatalysis.

In this work, we coupled SnO_2 nanoparticles with g-C_3N_4 to form different ratio composites and applied for the photocatalytic production of H_2 and 2-chlorophenol (2-CP) degradation under visible light, keeping in view to excite only g-C_3N_4 and use SnO_2 as excited charge acceptor. The optimized composite ($6SnO_2$/g-C_3N_4) showed much improved photoactivities for H_2 production and pollutant degradation compared to bare SnO_2 and g-C_3N_4. These activities are solely attributed to the better charge separation in the composites.

EXPERIMENTAL PART

Preparation of g-C_3N_4

Polymeric g-C_3N_4 was prepared from dicyandiamide. A given amount of dicyandiamide was taken in crucible and heated at 550°C in a muffle furnace for 4 h at the rate of 2°C/min. After the completion of the heating duration, the cooled sample was grinded into fine powder and used for further study.

Preparation of SnO_2 Nanoparticles

Chloride salt of Sn(IV) was dissolved in water, and the solution was made basic with the help of NaOH solution under vigorous stirring. During addition of NaOH, the solution initially became milky and then became clear with the addition of more NaOH. Finally, when the pH reached about 12, the solution was taken in an autoclave and heated at 220°C for 10 h in oven. The obtained white powder was purified three times with distilled water, dried in the oven overnight, and then calcined at 450°C for 1 h at the rate of 5°C/min.

Preparation of SnO_2/g-C_3N_4 Composites

Composites containing different mass percent of SnO_2 and g-C_3N_4 (SnO_2/g-C_3N_4) were prepared by taking appropriate amounts of SnO_2 and g-C_3N_4 in water–methanol mixture containing 1 ml of concentrated HNO_3. Each mixture was vigorously stirred under heating at 80°C till the whole solvent was evaporated. After that, each mixture was dried in the oven overnight and then calcined at 450°C for 1 h. The as prepared composites were represented by XSnO_2/g-C_3N_4 where "X" shows the percent amount (2, 4, 6, and 8%) of SnO_2 in the given composite.

Characterization Techniques

The prepared samples were passed through different characterization techniques to confirm the formation of heterojunctional composites. The X-ray diffraction (XRD) technique was used to determine the crystalline structure of the samples with the help of Bruker D8 Advance diffractometer using CuK_α radiation. The oxidation states of the constituent elements of the composites were examined by means of X-ray photoelectron spectroscopy (XPS) employing X-ray from mono-Al source with the help of a Kratos-Axis Ultra DLD apparatus. The obtained binding energies were calibrated with the binding energy of adventitious C-atom which is 284.55 eV. The microscopic structure was further revealed with the help of transmission electron microscope (TEM) and high-resolution TEM (HRTEM) operating at 200 kV. The optical properties were confirmed with the help of UV diffuse reflectance spectra, by taking $BaSO_4$ as a reference, measured with a Shimadzu UV-2550 spectrophotometer. The photoluminescence (PL) spectrum of each sample was realized with the help of spectrofluorophotometer (Perkin-Elmer LS55) at a 390-nm excitation wavelength. The steady state surface photovoltage spectroscopic (SS-SPS) measurement of each sample was carried in a controlled atmosphere employing a homemade equipment possessing a lock-in amplifier (SR830) synchronized with a light chopper (SR540). Each sample was first thoroughly grinded and then kept between two indium tin oxide (ITO) glass electrodes in an atmosphere-controlled sealed container. Radiations from a 500-W Xe lamp (CHF XQ500W, Global Xe lamp power) were passed through a double-prism monochromator (SBP300) to get a monochromatic light.

Evaluation of Photoactivity for Water Splitting

Water splitting photocatalysis was carried out with the help of an online H_2 production unit (Perfectlight, Beijing, Lab Solar III). About 0.1 g photocatalyst was taken in a glass-made reaction cell, and 100-ml aqueous solution of methanol (20% V/V) was added. The apparatus was first deaerated with the help of a vacuum pump to remove any traces of O_2 and CO_2 dissolved

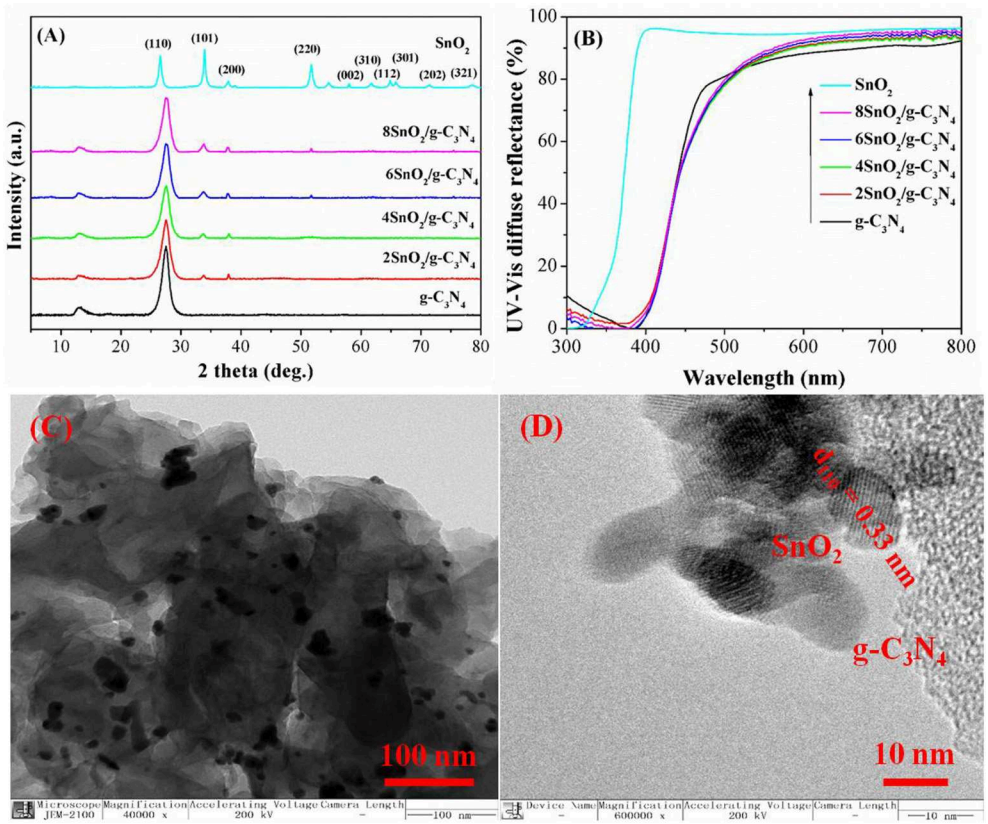

FIGURE 1 | X-ray diffraction (XRD) pattern **(A)** and diffuse reflectance spectroscopy (DRS) **(B)** of g-C_3N_4, SnO_2, and $XSnO_2$/g-C_3N_4. Transmission electron microscope (TEM) image **(C)** and high-resolution TEM (HRTEM) images **(D)** of $6SnO_2$/g-C_3N_4.

in aqueous solution. The mixture was irradiated under visible light (wavelength > 420 nm) coming from a 300-W Xe lamp under vigorous stirring. The produced gases were analyzed after each hour with the help of a gas chromatograph (7,900, TCD, molecular sieve 5 Å, N_2 carrier, Tec comp.).

Evaluation of Photoactivity for Pollutant Degradation

The photoactivities were further studied by selecting 2-CP as a pollutant. About 0.2 g of powder sample was mixed with 50 ml of aqueous solution (25 mg/L) of 2-CP and exposed to a 150-W (GYZ220) Xe lamp under visible light (wavelength > 420 nm). Before being exposed to light, each sample was first kept in complete dark for 30 min to attain adsorption–desorption equilibrium. The concentration of the pollutant was checked after each hour with the help of a Shimadzu UV-2550 spectrometer.

Evaluation of Hydroxyl Radicals (·OH)

About 0.05 g powder sample was mixed with 50 ml of aqueous solution of coumarin (0.001 M) and exposed to a 150-W (GYZ220) Xe lamp under visible light (wavelength > 420 nm). Before exposure to light, each sample was first kept in complete dark for 30 min to attain adsorption–desorption equilibrium. After each hour, the amount of formed 7-hydroxycoumarin was checked at 390-/460-nm excitation/emission wavelengths with the help of a spectrofluorophotometer (Perkin-Elmer LS55).

RESULT AND DISCUSSION

Structural Characterization

The crystal structure study of the pure g-C_3N_4 shows two characteristic diffraction peaks at 13.04 and 27.31° as shown in **Figure 1A**. The former peak is due to the interplanner stacking of the aromatic rings in conjugation while the later peak is related to the interlayer structural units (Liu et al., 2017; Guan et al., 2018; Xu et al., 2018b, 2019b). Similarly, pure SnO_2 shows diffraction peaks at 26.2, 33.8, 37.3, 51.2, 57.2, 61.1, 63.81, 64.77, 71.38, and 78.27°, which can be, respectively, indexed to (110), (101), (200), (220), (002), (310), (112), (301), (202), and (321) planes of tetragonal SnO_2 nanoparticles (Mahjouri et al., 2020; Shokrzadeh et al., 2020). Interestingly, all the composite samples show the two characteristic peaks of g-C_3N_4 at 13.04 and 27.31° and SnO_2 peaks at 33.8, 37.3, and 51.2°. However, the diffraction peak at 13.04° has been decreased progressively as the amount of SnO_2 is increased, indicating that SnO_2 nanoparticles are well packed in the nanosheets of g-C_3N_4.

The UV-vis diffused reflectance spectra of the samples are shown in **Figure 1B**. As can be seen, g-C_3N_4 and SnO_2,

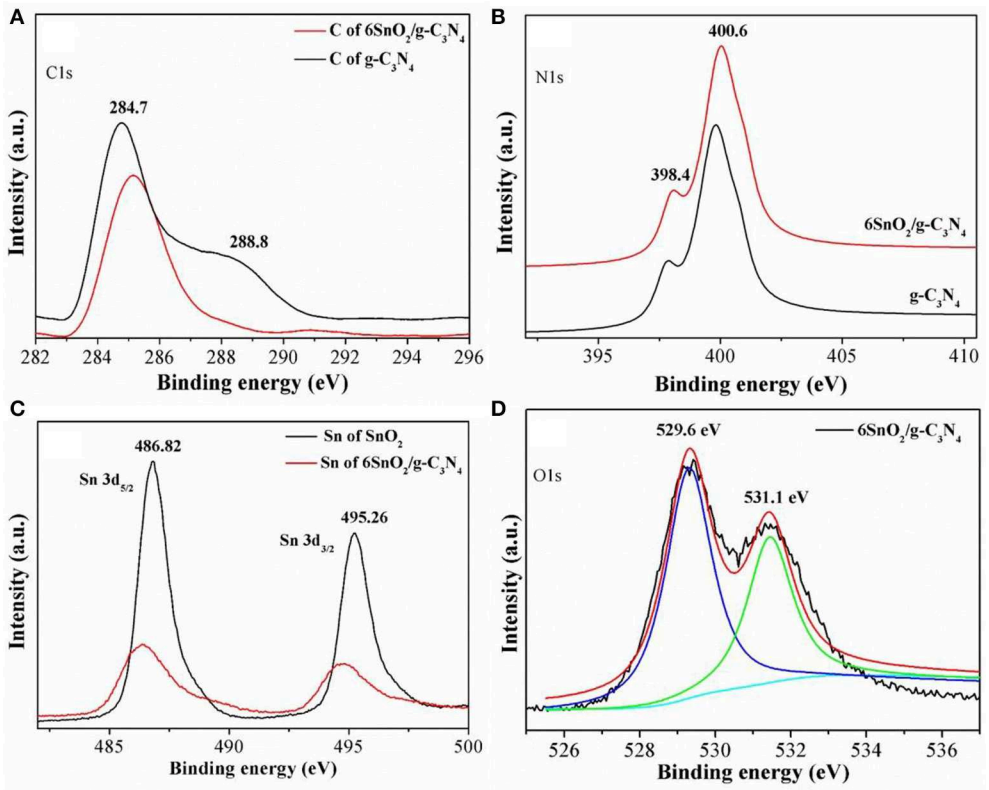

FIGURE 2 | X-ray photoelectron spectra of C1s **(A)**, N1s **(B)**, Sn 3d **(C)**, and O1s **(D)** of g-C_3N_4 and SnO_2.

respectively, show optical thresholds at 475 and 360 nm, corresponding to band gaps of 2.61 and 3.45 eV, respectively. Although the composite samples show the same optical thresholds at 475 and 360 nm, their light absorption has been slightly decreased as SnO_2 is a wide-band-gap semiconductor and its coupling with g-C_3N_4 slightly decreases light absorption (Zhang et al., 2018; Zada et al., 2019a; Zhu et al., 2019a,b).

The TEM image of composite shows uniform distribution of small SnO_2 nanoparticles of about 10-nm size on the surface of g-C_3N_4 as shown in **Figure 1C**. The HRTEM image shows the lattice fringes of 0.33-nm interplanar distance corresponding to the (110) plane of SnO_2 (**Figure 1D**). This shows that both g-C_3N_4 and SnO_2 are in close contact with each other to intensify the charge separation for better photoactivities.

The oxidation states of different elements in the samples were determined using XPS measurements, and the results are shown in **Figure 2**. The obtained binding energies were calibrated with the binding energy of the adventitious carbon atom with a binding energy value of 284.55 eV. It is obvious that C1s in pure g-C_3N_4 shows two XPS peaks at binding energies of 284.7 and 288.2 eV (**Figure 2A**). These peaks are attributed to the sp^2 hybridized C-atoms, respectively, bonded with N-atom of the aromatic ring and NH_2 group linking different aromatic rings. Similarly, the XPS binding energies of N1s in pure g-C_3N_4 are composed of two parts at 398.4 and 400.6 eV and are, respectively, contributed by sec. and ter. N-atoms (**Figure 2B**) (Raziq et al., 2016; Li Q. et al., 2019). The XPS peaks of Sn in pure SnO_2 are deconvoluted into two parts at 486.82 and 495.26 eV, which are, respectively, contributed by $Sn3d_{5/2}$ and $Sn3d_{3/2}$ and show that Sn is present in +4 oxidation state in the nanocomposite (**Figure 2C**) (Li H. et al., 2019). When g-C_3N_4 nanosheets are coupled with SnO_2 nanoparticles, the C1s and N1s peaks are slightly shifted toward the low-energy side while those of Sn are shifted toward the high-energy side. The binding energies of O1s in **Figure 2D** are contributed at 529.6 and 531.1 eV, which are, respectively, contributed by the lattice O-atom and adsorbed oxygen molecules. The redistribution of charge density in both components of the nanocomposite indicates that both g-C_3N_4 and SnO_2 are present in close contact with each other for improved charge separation.

Photocatalytic Activity

The photoactivities of composites were first evaluated by splitting water under visible light (wavelength > 420 nm) in the presence of methyl alcohol. As shown in the **Figure 3A**, the H_2 production activity of pure SnO_2 is negligible under visible light irradiation. However, pure g-C_3N_4 produces about 10 μmol of H_2 in 1 h under the stipulated conditions. Interestingly, these H_2 photoactivities are significantly enhanced when both g-C_3N_4 and SnO_2 are coupled to form heterojunctional composites. Further, photoactivities are increased along with the increase in the amount of SnO_2 nanoparticles and the highest activities are

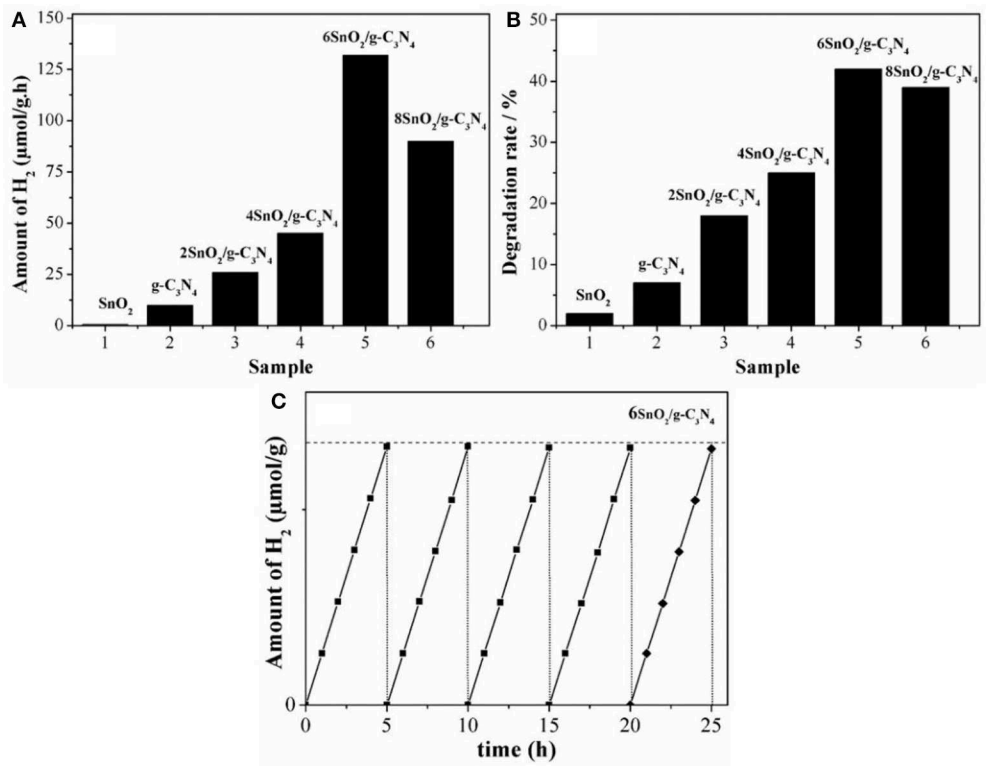

FIGURE 3 | Photoactivities for H_2 evolution **(A)**, 2-CP degradation **(B)** of pure g-C_3N_4, and XSnO_2/g-C_3N_4 and stability test of 6SnO_2/g-C_3N_4 **(C)**.

contributed by 6SnO_2/g-C_3N_4 sample, which are 132 μmol/h. However, further increase in the amount of SnO_2 decreases H_2 production as SnO_2 is a wide-band-gap semiconductor and it covers most surface of the g-C_3N_4 to prevent absorption of visible-light photons. These enhanced H_2 activities are solely attributed to the improved charge separation in the composites by transferring excited electrons from g-C_3N_4 to SnO_2 for the reduction of water. We further extended the photoactivities by measuring the degradation of 2-CP under visible-light (wavelength > 420 nm) irradiation. Again, the degradation performance of pure SnO_2 is very low due to its high-band-gap nature. The composite materials showed much improved photoactivities, and the optimized 6SnO_2/g-C_3N_4 sample showed 42% degradation activities under the given conditions as shown in **Figure 3B**. We also carried out the stability test of the optimized sample for five consecutive cycles, each cycle composed of a 5-h run. It is obvious from **Figure 3C** that there is no detectable decrease in the H_2 production activities, indicating that the optimized sample is very stable.

Charge Separation

The improved photoactivities of the composites compared to pure g-C_3N_4 are attributed to the extended charge separation. In order to determine it, we carried out PL spectra, keeping excitation λ at 390 nm. It is clear from **Figure 4A** that g-C_3N_4 gives intense peak at 470 nm, indicating poor charge separation. However, the intensities of the composites are progressively decreased as the amount of SnO_2 nanoparticles is increased, and the optimized sample shows relatively low PL peak, indicating excellent charge separation in it (Zhang et al., 2015; Ali et al., 2016; Lu et al., 2018; Ali N. et al., 2019; Ali S. et al., 2019). The relatively low intensities of PL peaks indicate enhanced charge separation and are responsible for improved photoactivities.

We further extended the charge separation experiments by measuring the atmosphere-controlled steady state surface photovoltage spectra (SS-SPS), and the results are shown in **Figure 4B**. As evident, g-C_3N_4 shows very low SPS intensity. However, the SPS peak intensities are much improved when both g-C_3N_4 and SnO_2 are coupled and the optimized 6SnO_2/g-C_3N_4 sample shows the highest peak intensity. Since high is the intensity of the SPS peak, high is the charge separation (Zada et al., 2018, 2019a,b); therefore, we can say that the composites impart enhanced charge separation and contributing to the improved photoactivities.

We also measured the hydroxyl radical (·OH) activities of the fabricated samples by doing coumarin fluorescent experiments under visible-light irradiation. Since ·OH is the major contributor to charge separation during photocatalysis and react with coumarin to form 7-hydroxycoumarin; therefore, the higher the intensity of coumarin fluorescent peak, the higher is the charge separation. As can be seen from **Figure 4C**, pure

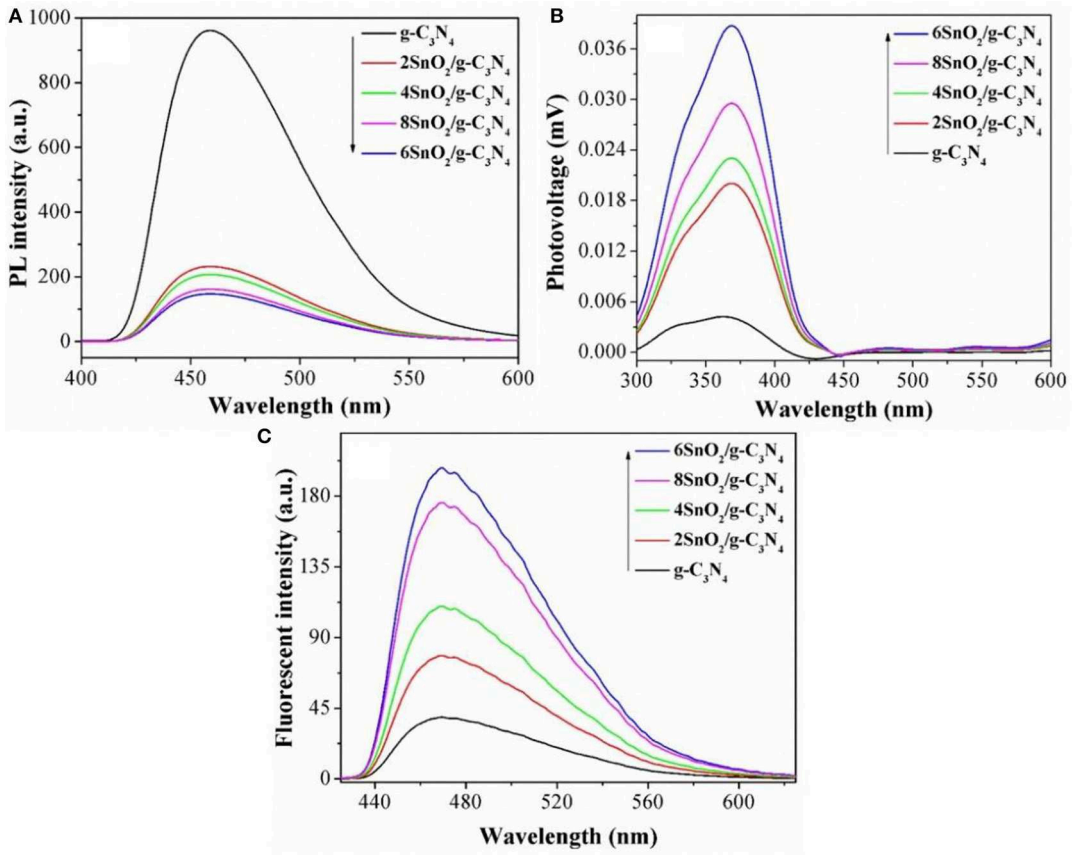

FIGURE 4 | Photoluminescence spectra **(A)**, SS-SPS **(B)**, and coumarin fluorescent spectra **(C)** of pure g-C_3N_4 and XSnO_2/g-C_3N_4.

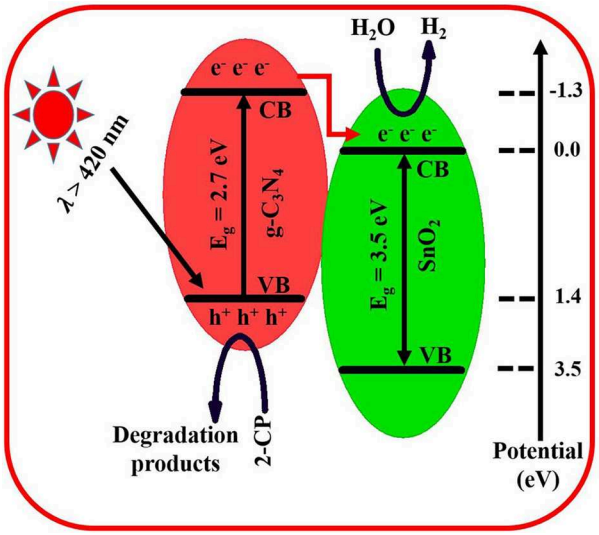

FIGURE 5 | Schematic representation of charge separation, H_2 production, and pollutant degradation by 6SnO_2/g-C_3N_4.

g-C_3N_4 gives very low peak, which shows its inherited low charge separation. However, the ·OH radical activities are considerably improved when both g-C_3N_4 and SnO_2 are coupled, indicating improved charge separation and hence extended photoactivities (Ali et al., 2018a; Yasmeen et al., 2019a).

DISCUSSION

The improved charge separation in the prepared composite results in the enhanced H_2 production and 2-CP degradation. This enhanced charge separation has been schematically shown in **Figure 5**. The band gap of g-C_3N_4 is about 2.7 eV and absorbs visible-light photons (Raziq et al., 2015, 2017). Its CB present at −1.3 eV is most suitable for H_2 production and superoxide generation which require reduction potential of 0.00 and −0.33 eV, respectively. Its VB is present at 1.4 eV (Yasmeen et al., 2019b). On the other side, the band gap of SnO_2 is 3.5 eV, and its CB is present below the CB of g-C_3N_4 (Zada et al., 2016). Under visible-light irradiation, only g-C_3N_4 is excited, and electrons jumped to its CB, leaving positive holes in the VB. Since the excited electrons have a very short lifetime; therefore, they jumped to the CB of SnO_2 to achieve some stability for a while. Here these electrons reduce water into H_2 while the holes in VB of g-C_3N_4 are solely left to carryout oxidation of alcohol. In case of 2-CP degradation, these positive holes either directly oxidize pollutants or undergo the formation of more reactive species such as hydroxyl-free radicals, which then finally degrade the target pollutant into simple CO_2 and water (Zada et al., 2018).

CONCLUSION

In order to overcome energy crises and environmental pollution, here, we synthesized g-C_3N_4 nanosheets and coupled them with SnO_2 nanoparticles. The optimized composite of 6SnO_2/g-C_3N_4 produced about 132 μmol of H_2 from water in 1 h and degraded 42% 2-CP pollutant under visible-light irradiation as compared to the photoactivities of bare g-C_3N_4 and SnO_2. These enhanced photoactivities are attributed to the better charge separation as the excited electrons thermodynamically transfer from g-C_3N_4 to SnO_2 as has been confirmed from photoluminescence spectra, steady state surface photovoltage spectroscopic measurement, and formed hydroxyl radicals. It is believed that this work would provide a feasible route to synthesize photocatalysts for improved energy production and environmental purification.

DATA AVAILABILITY STATEMENT

The raw data supporting the conclusions of this article will be made available by the authors, without undue reservation, to any qualified researcher.

AUTHOR CONTRIBUTIONS

All authors listed have made a substantial, direct and intellectual contribution to the work, and approved it for publication.

FUNDING

This work was supported by the Doctoral Scientific Research Foundation of Liaoning Province (20170520011) and Project of Education Office of Liaoning Province (LQN201712).

REFERENCES

Ali, A., Hussain, Z., Arain, M. B., Shah, N., Khan, K. M., Gulab, H., et al. (2016). Development of microwave assisted spectrophotometric method for the determination of glucose. *Spectrochim. Acta Mol. Biomol. Spectrosc.* 153, 374–378. doi: 10.1016/j.saa.2015.07.104

Ali, N., Awais, K. T., Ul-Islam, Khan, M. A., Shah, S. J., and Zada, A. (2018b). Chitosan-coated cotton cloth supported copper nanoparticles for toxic dye reduction. *Int. J. Biol. Macromol.* 111, 832–838. doi: 10.1016/j.ijbiomac.2018.01.092

Ali, N., Zada, A., Zahid, M., Ismail, A., Rafiq, M., Riaz, A., et al. (2019). Enhanced photodegradation of methylene blue with alkaline and transition-metal ferrite nanophotocatalysts under direct sun light irradiation. *J. Chin. Chem. Soc.* 66, 402–408. doi: 10.1002/jccs.201800213

Ali, S., Li, Z., Chen, S., Zada, A., Khan, I., Khan, I., et al. (2019). Synthesis of activated carbon-supported TiO_2-based nano-photocatalysts with well recycling for efficiently degrading high-concentration pollutants. *Catal. Today* 335, 557–564. doi: 10.1016/j.cattod.2019.03.044

Ali, W., Ullah, H., Zada, A., Alamgir, M. K., Muhammad, W., Ahmad, M. J., et al. (2018a). Effect of calcination temperature on the photoactivities of ZnO/SnO_2 nanocomposites for the degradation of methyl orange. *Mater. Chem. Phys.* 213, 259–266. doi: 10.1016/j.matchemphys.2018.04.015

Dong, D., Yan, C., Huang, J., Lu, N., Wu, P., Wang, J., et al. (2019). An electron-donating strategy to guide the construction of MOF photocatalysts toward co-catalyst-free highly efficient photocatalytic H_2 evolution. *J. Mater. Chem. A* 7, 24180–24185. doi: 10.1039/C9TA06141J

Fu, J., Xu, Q., Low, J., Jiang, C., and Yu, J. (2019). Ultrathin 2D/2D WO_3/g-C_3N_4 step-scheme H_2-production photocatalyst. *Appl. Catal. B Environ.* 243, 556–565. doi: 10.1016/j.apcatb.2018.11.011

Gautam, S., Shandilya, P., Singh, V. P., Raizada, P., and Singh, P. (2016). Solar photocatalytic mineralization of antibiotics using magnetically separable $NiFe_2O_4$ supported onto graphene sand composite and bentonite. *J. Water Process Eng.* 14, 86–100. doi: 10.1016/j.jwpe.2016.10.008

Guan, W., Zhang, Z., Tian, S., and Du, J. (2018). Ti_4O_7/g-C_3N_4 for visible light photocatalytic oxidation of hypophosphite: effect of mass ratio of Ti_4O_7/g-C_3N_4. *Front. Chem.* 6:313. doi: 10.3389/fchem.2018.00313

Jana, S., and Mondal, A. (2014). Fabrication of SnO_2/α-Fe_2O_3, SnO_2/α-Fe_2O_3-PB heterostructure thin films: enhanced photodegradation and peroxide sensing. *ACS Appl. Mater. Interfaces* 6, 15832–15840. doi: 10.1021/am5030879

Li, F., Wangyang, P., Zada, A., Humayun, M., Wang, B., and Qu, Y. (2016). Synthesis of hierarchical Mn_2O_3 microspheres for photocatalytic hydrogen production. *Mater. Res. Bull.* 84, 99–104. doi: 10.1016/j.materresbull.2016.07.032

Li, H., Zhang, B., Wang, X., Zhang, J., An, T., Ding, Z., et al. (2019). Heterostructured SnO_2-SnS_2@C embedded in nitrogen-doped graphene as a robust anode Material for lithium-ion batteries. *Front. Chem.* 7:339. doi: 10.3389/fchem.2019.00339

Li, Q., Shi, T., Li, X., Lv, K., Li, M., Liu, F., et al. (2018a). Remarkable positive effect of $Cd(OH)_2$ on CdS semiconductor for visible-light photocatalytic H_2 production. *Appl. Catal. B: Environ.* 229, 8–14. doi: 10.1016/j.apcatb.2018.01.078

Li, Q., Xia, Y., Yang, C., Lv, K., Lei, M., and Li, M. (2018b). Building a direct Z-scheme heterojunction photocatalyst by $ZnIn_2S_4$ nanosheets and TiO_2 hollow spheres for highly-efficient artificial photosynthesis. *Chem. Eng. J.* 349, 287–296. doi: 10.1016/j.cej.2018.05.094

Li, Q., Zhao, T., Li, M., Li, W., Yang, B., Qin, D., et al. (2019). One-step construction of Pickering emulsion via commercial TiO_2 nanoparticles for photocatalytic dye degradation. *Appl. Catal. B Environ.* 249, 1–8. doi: 10.1016/j.apcatb.2019.02.057

Liu, C., Raziq, F., Li, Z., Qu, Y., Zada, A., and Jing, L. (2017). Synthesis of TiO_2/g-C_3N_4 nanocomposites with phosphate-oxygen functional bridges for improved photocatalytic activity. *Chin. J. Catal.* 38, 1072–1078. doi: 10.1016/S1872-2067(17)62850-X

Liu, M., Wageh, S., Al-Ghamdi, A. A., Xia, P., Cheng, B., Zhang, L., et al. (2019). Quenching induced hierarchical 3D porous g-C_3N_4 with enhanced photocatalytic CO_2 reduction activity. *Chem. Commun.* 55, 14023–14026. doi: 10.1039/C9CC07647F

Liu, Y., Zhang, Z., Fang, Y., Liu, B., Huang, J., Miao, F., et al. (2019). IR-Driven strong plasmonic-coupling on Ag nanorices/$W_{18}O_{49}$ nanowires heterostructures for photo/thermal synergistic enhancement of H_2 evolution from ammonia borane. *Appl. Catal. B Environ.* 252, 164–173. doi: 10.1016/j.apcatb.2019.04.035

Lu, N., Zhang, Z., Wang, Y., Liu, B., Guo, L., Wang, L., et al. (2018). Direct evidence of IR-driven hot electron transfer in metal-free plasmonic $W_{18}O_{49}$/Carbon heterostructures for enhanced catalytic H_2 production. *Appl. Catal. B Environ.* 233, 19–25. doi: 10.1016/j.apcatb.2018.03.073

Mahjouri, S., Nasab, M. K., Kazemi, E. M., Divband, B., and Movafeghi, A. (2020). Effect of Ag-doping on cytotoxicity of SnO_2 nanoparticles in tobacco cell cultures. *J. Hazard. Mater.* 381:121012. doi: 10.1016/j.jhazmat.2019.121012

Nie, N., Zhang, L., Fu, J., Cheng, B., and Yu, J. (2018). Self-assembled hierarchical direct Z-scheme g-C_3N_4/ZnO microspheres with enhanced photocatalytic CO_2 reduction performance. *Appl. Surf. Sci.* 441, 12–22. doi: 10.1016/j.apsusc.2018.01.193

Qi, K., Li, Y., Xie, Y., Liu, S., Zheng, K., Chen, Z., et al. (2019a). Ag loading enhanced photocatalytic activity of g-C_3N_4 porous nanosheets for decomposition of organic pollutants. *Front. Chem.* 7:91. doi: 10.3389/fchem.2019.00091

Qi, K., Liu, S., Chen, Y., Xia, B., and Li, G. (2018b). A simple post-treatment with urea solution to enhance the photoelectric conversion efficiency for TiO_2 dye-sensitized solar cells. *Sol. Energy Mater. Sol. Cells* 183, 193–199. doi: 10.1016/j.solmat.2018.03.038

Qi, K., Liu, S., and Qiu, M. (2018a). Photocatalytic performance of TiO_2 nanocrystals with/without oxygen defects. *Chin. J. Catal.* 39, 867–875. doi: 10.1016/S1872-2067(17)62999-1

Qi, K., Liu, S., Selvaraj, R., Wang, W., and Yan, Z. (2019b). Comparison of Pt and Ag as co-catalyst on g-C_3N_4 for improving photocatalytic activity: experimental and DFT studies. *Desalination Water Treat.* 153, 244–252. doi: 10.5004/dwt.2019.24079

Qi, K., Liu, S., Wang, R., Chen, Z., and Selvaraj, R. (2019c). Pt/g-C_3N_4 composites for photocatalytic H_2 production and $^{\cdot}OH$ formation. *Desalination Water Treat*. 154, 312–319. doi: 10.5004/dwt.2019.24068

Qi, K., Lv, W., Khan, I., and Liu, S. (2020a). Photocatalytic H_2 generation via CoP quantum-dot-modified g-C_3N_4 from electroless plating synthesis. *Chin. J. Catal*. 41, 114–121. doi: 10.1016/S1872-2067(19)63459-5

Qi, K., Xie, Y., Wang, R., Liu, S., and Zhao, Z. (2019d). Electroless plating Ni-P cocatalyst decorated g-C_3N_4 with enhanced photocatalytic water splitting for H_2 generation. *Appl. Surf. Sci.* 466, 847–853. doi: 10.1016/j.apsusc.2018.10.037

Qi, K., Xing, X., Zada, A., Li, M., Wang, Q., Liu, S., et al. (2020b). Transition metal doped ZnO nanoparticles with enhanced photocatalytic and antibacterial performances: experimental and DFT studies. *Ceram. Int*. 46, 1494–1502. doi: 10.1016/j.ceramint.2019.09.116

Qu, Y., Sun, N., Humayun, M., Zada, A., Xie, Y., Tang, J., et al. (2018). Improved visible-light activities of nanocrystalline CdS by coupling with ultrafine NbN with lattice matching for hydrogen evolution. *Sustainable Energy Fuels* 2, 549–552. doi: 10.1039/C7SE00610A

Raizada, P., Kumari, J., Shandilya, P., and Singh, P. (2017). Kinetics of photocatalytic mineralization of oxytetracycline and ampicillin using activated carbon supported ZnO/$ZnWO_4$ nanocomposite in simulated wastewater. *Desalination Water Treat*. 79, 204–213. doi: 10.5004/dwt.2017.20831

Ran, J., Guo, W., Wang, H., Zhu, B., Yu, J., and Qiao, S. (2018). Metal-free 2D/2D phosphorene/g-C_3N_4 Van der Waals heterojunction for highly enhanced visible-light photocatalytic H_2 production. *Adv. Mater.* 30, 1800128. doi: 10.1002/adma.201800128

Raziq, F., Li, C., Humayun, M., Qu, Y., Zada, A., Yu, H., et al. (2015). Synthesis of TiO_2/g-C_3N_4 nanocomposites as efficient photocatalysts dependent on the enhanced photogenerated charge separation. *Mater. Res. Bull.* 70, 494–499. doi: 10.1016/j.materresbull.2015.05.018

Raziq, F., Qu, Y., Humayun, M., Zada, A., Yu, H., and Jing, L. (2017). Synthesis of SnO_2/B-P codoped g-C_3N_4 nanocomposites as efficient cocatalyst-free visible-light photocatalysts for CO_2 conversion and pollutant degradation. *Appl. Catal. B Environ.* 201, 486–494. doi: 10.1016/j.apcatb.2016.08.057

Raziq, F., Qu, Y., Zhang, X., Humayun, M., Wu, J., Zada, A., et al. (2016). Enhanced cocatalyst-free visible-light activities for photocatalytic fuel production of g-C_3N_4 by trapping holes and transferring electrons. *J. Phys. Chem. C* 120, 98–107. doi: 10.1021/acs.jpcc.5b10313

Shokrzadeh, L., Mohammadi, P., Mahmoudian, M. R., Basirun, W. J., and Bahreini, M. (2020). L-glycine-assisted synthesis of SnO_2/Pd nanoparticles and their application in detection of biodeteriorating fungi. *Mater. Chem. Phys*. 240:122172. doi: 10.1016/j.matchemphys.2019.122172

Singh, P., Gautam, S., Shandilya, P., Priya, B., Singh, V. P., and Raizada, P. (2017). Graphene bentonite supported $ZnFe_2O_4$ as superparamagnetic photocatalyst for antibiotic degradation. *Adv. Mater. Lett.* 8, 229–238. doi: 10.5185/amlett.2017.1467

Ullah, M., Nazir, R., Khan, M., Khan, W., Shah, M., Afridi, S. G., et al. (2019). Effective removal of heavy metals from water by activated carbon adsorbents of Albizia lebbeck and Melia azedarach seed shells. *Soil Water Res.* 15, 30–37. doi: 10.17221/212/2018-SWR

Wang, J., Qin, C., Wang, H., Chu, M., Zada, A., Zhang, X., et al. (2018). Exceptional photocatalytic activities for CO_2 conversion on Al-O bridged g-C_3N_4/α-Fe_2O_3 Z-scheme nanocomposites and mechanism insight with isotopesz. *Appl. Catal. B Environ.* 221, 459–466. doi: 10.1016/j.apcatb.2017.09.042

Xu, B., Zada, A., Wang, G., and Qu, Y. (2019a). Boosting the visible-light photoactivities of $BiVO_4$ nanoplates by doping Eu and coupling CeO_x nanoparticles for CO_2 reduction and organic oxidation. *Sust. Energy Fuels* 3, 3363–3369. doi: 10.1039/C9SE00409B

Xu, D., Cheng, B., Wang, W., Jiang, C., and Yu, J. (2018a). Ag_2CrO_4/g-C_3N_4/graphene oxide ternary nanocomposite Z-scheme photocatalyst with enhanced CO_2 reduction activity. *Appl. Catal. B Environ.* 231, 368–380. doi: 10.1016/j.apcatb.2018.03.036

Xu, Q., Zhu, B., Cheng, B., Yu, J., Zhou, M., and Ho, W. (2019b). Photocatalytic H_2 evolution on graphdiyne/g-C_3N_4 hybrid nanocomposites. *Appl. Catal. B Environ.* 255:117770. doi: 10.1016/j.apcatb.2019.117770

Xu, Q., Zhu, B., Jiang, C., Cheng, B., and Yu, J. (2018b). Constructing 2D/2D Fe_2O_3/g-C_3N_4 direct Z-scheme photocatalysts with enhanced H_2 generation performance. *Sol. PRL* 2:1800006. doi: 10.1002/solr.201800006

Yasmeen, H., Zada, A., Li, W., Xu, M., and Liu, S. (2019b). Suitable energy platform of Bi_2WO_6 significantly improves visible-light degradation activity of g-C_3N_4 for highly toxic diuron pollutant. *Mater. Sci. Semicond. Process.* 102:104598. doi: 10.1016/j.mssp.2019.104598

Yasmeen, H., Zada, A., and Liu, S. (2019a). Dye loaded MnO_2 and chlorine intercalated g-C_3N_4 coupling impart enhanced visible light photoactivities for pollutants degradation. *J. Photochem. Photobiol. A Chem.* 380:111867. doi: 10.1016/j.jphotochem.2019.111867

Zada, A., Ali, N., Subhan, F., Anwar, N., Shah, M. I. A., Ateeq, M., et al. (2019a). Suitable energy platform significantly improves charge separation of g-C_3N_4 for CO_2 reduction and pollutant oxidation under visible-light. *Prog. Nat. Sci. Mat. Int.* 29, 138–144. doi: 10.1016/j.pnsc.2019.03.004

Zada, A., Humayun, M., Raziq, F., Zhang, X., Qu, Y., Bai, L., et al. (2016). Exceptional visible-light-driven cocatalyst-free photocatalytic activity of g-C_3N_4 by well-designed nanocomposites with plasmonic Au and SnO_2. *Adv. Energy Mater.* 6:1601190, doi: 10.1002/aenm.201601190

Zada, A., Muhammad, P., Ahmad, W., Hussain, Z., Ali, S., Khan, M., et al. (2019b). Surface plasmonic-assisted photocatalysis and optoelectronic devices with noble metal nanocrystals: design, synthesis, and applications. *Adv. Funct. Mater*. 6:1906744. doi: 10.1002/adfm.201906744

Zada, A., Qu, Y., Ali, S., Sun, N., Lu, H., Yan, R., et al. (2018). Improved visible-light activities for degrading pollutants on TiO_2/g-C_3N_4 nanocomposites by decorating SPR Au nanoparticles and 2,4-dichlorophenol decomposition path. *J. Hazard. Mater.* 342, 715–723. doi: 10.1016/j.jhazmat.2017.09.005

Zhang, Z., Huang, J., Zhang, M., Yuan, Q., and Dong, B. (2015). Ultrathin hexagonal SnS_2 nanosheets coupled with g-C_3N_4 nanosheets as 2D/2D heterojunction photocatalysts toward high photocatalytic activity. *Appl. Catal. B Environ.* 163, 298–305. doi: 10.1016/j.apcatb.2014.08.013

Zhang, Z., Jiang, X., Liu, B., Guo, L., Lu, N., Wang, L., et al. (2018). IR-driven ultrafast transfer of plasmonic hot electrons in nonmetallic branched heterostructures for enhanced H_2 generation. *Adv. Funct. Mater*. 30:1705221. doi: 10.1002/adma.201705221

Zhao, X., Zhang, J., Wang, B., Zada, A., and Humayun, M. (2015). Biochemical synthesis of Ag/AgCl nanoparticles for visible-light-driven photocatalytic removal of colored dyes. *Materials* 8, 2043–2053. doi: 10.3390/ma8052043

Zhu, B., Cheng, B., Zhang, L., and Yu, J. (2019a). Review on DFT calculation of s-triazine-based carbon nitride. *Carbon Energy* 1, 32–56. doi: 10.1002/cey2.1

Zhu, B., Wageh, S., Al-Ghamdi, A. A., Yang, S., Tian, Z., and Yu, J. (2019b). Adsorption of CO_2, O_2, NO and CO on s-triazine-based g-C_3N_4 surface. *Catal. Today* 335, 117–127. doi: 10.1016/j.cattod.2018.09.038

Zhu, Y., Zhang, Z., Lu, N., Hua, R., and Dong, B. (2019c). Prolonging charge-separation states by doping lanthanide-ions into {001}/{101} facets-coexposed TiO_2 nanosheets for enhancing photocatalytic H_2 evolution. *Chin. J. Catal.* 40, 413–423. doi: 10.1016/S1872-2067(18)63182-1

Conflict of Interest: The authors declare that the research was conducted in the absence of any commercial or financial relationships that could be construed as a potential conflict of interest.